Reaction-Path Dynamics Calculations Using Integrated Methods. The CF_3CH_3 + OH Hydrogen Abstraction Reaction

J. Espinosa-García†

Departamento de Química Física, Universidad de Extremadura, 06071 Badajoz, Spain

Received: December 18, 2001; In Final Form: March 19, 2002

The titlte reaction is used as a test to analyze the performance of the integrated methods by describing the intrinsic reaction path and then calculating kinetic and dynamic information for reactions involving the breaking−forming of covalent bonds in large molecules. The integrated methods split the "complete" system into two parts or layers and apply different levels of theory to each, which is especially interesting for the treatment of large molecules. We located and characterized the stationary points (reactants, products, and saddle point), calculated the energy, gradient, and Hessian along the intrinsic reaction path, and then, with this information, calculated thermal rate constants for the temperature range 250−500 K, using variational transition-state theory and multidimensional tunneling effect. The integrated method used (IMOMO) reproduces the values of the high-level method, corrects the deficiencies of the low-level method, and represents a substantial saving in computational cost. Its success is related to the higher-level description of the "model" system or inner layer (CH_4 + OH, in this case), with the effect of the lower-level description of the outer layer being smaller. The analysis of the coupling between the reaction coordinate and normal modes along the reaction path showed that the vibrational excitation of the reactive C−H stretching mode can enhance the forward rate constant and that the H_2O normal modes (stretching and bending) can appear vibrationally excited in the exit channel. Variational effects and tunneling were found to be important, a behavior already known for the "model" system. Although we used high ab initio electronic levels, our theoretical rate constants markedly underestimate the experimental values. This problem arises from only partially introducing the correlation energy and using incomplete basis sets, a general problem in computational chemistry, and it is not directly related to the integrated method used here.

1. Introduction

Even today, the complete construction of the potential energy surface (PES) of a polyatomic system is a prohibitive task, and several alternatives have been proposed to solve this problem. An interesting and successful alternative is the "direct dynamics" approach,[1−3] which describes a chemical reaction by using electronic structure calculations (energies, gradients and Hessians) without the mediation of a PES fit.The method is especially powerful when combined with dynamics methods that require PES information only in the region of configuration space along the reaction path. The major limitation of this approach is its high computational cost, which obviously increases with the molecular size.

One economical approach involves density functional theory (DFT).[4−8] While the ab initio electronic structure calculations (with electron correlation) scale, at least, as N,[5] where N is the number of basis functions, DFT calculations scale as N^3, with the consequent computational saving. It is well-known that DFT calculations or hybrid DFT calculations that mix in some Hartree−Fock exchange yield reasonable geometries and vibrational frequencies,[9] atomization energies, [10] and enthalpies of formation.[11] However, when breaking−forming bonds are involved in the transition-state zone, DFT fails to perform well,[12−20] and generally underestimates the barrier height by several kcal mol^{-1}. For instance, Proynov et al.[19] analyzed the performance of several DFT methods with the much studied H + H_2 system, and found that all DFT and hybrid DFT calculations underestimate the barrier height by several kcal mol^{-1}, with the popular B3LYP calculation giving an error of 4.1 kcal mol^{-1}. A more exhaustive study was performed by Lynch and Truhlar[20] on a set of 22 reactions. In general, they found that the DFT and hybrid DFT methods underestimate the barrier height by about 3.4 kcal mol^{-1}, with one method (MPW1K: modified Perdew−Wang 1-parameter-method for kinetics) parametrized by the authors[21] themselves, predicting the most accurate saddle-point geometries and a mean unsigned error of only 1.5 kcal mol^{-1} for either basis set analyzed. Note that for this same set of 22 reactions, the MP2 (second-order Møller−Plasset perturbation theory) ab initio level has a mean error of 5.8 kcal mol^{-1}, and the more expensive QCISD (quadratic configuration interaction with single and double excitations) ab initio level has a mean error of 3.5 kcal mol^{-1}, indicating the necessity to use highly correlated wave functions and large basis sets. The accuracy limitation of the DFT and hybrid DFT approaches dissuade one from using them for the reaction-path description.

An interesting and economic group of alternatives for the problem of large molecules and high-level calculations are the integrated methods, which describe different parts of the large system with different theoretical approaches. The main goal is to reproduce the results of a high-level theoretical calculation for a large, "complete" system, by dividing it into two parts: a small "model" system (which is the most active site, where the breaking−forming bonds are involved), and the "rest" of the

† E-mail: joaquin@unex.es.

10.1021/jp0145513 CCC: $22.00
Published on Web 05/16/2002

molecular system. Different levels of theory are applied to these two parts, a higher level for the "model" system and a lower level for the "complete" system. Beginning with the pioneer work of Warshel and Levitt[22] in 1976, considerable effort has been devoted in this direction.[22−39] The first studies were devoted to the analysis of stationary points with special attention to stable molecules. Thus, Morokuma and co-workers[27−33,39] developed a number of useful strategies in this field. At a first step, they combined quantum mechanical (QM) (for the "model" system) and molecular mechanics (MM) (for the "complete" system) descriptions, and the method was denoted IMOMM[29] (integrated ab initio molecular orbital-molecular mechanics). Later, they developed the IMOMO method[30] (integrated ab initio molecular orbital-molecular orbital) where the "model" and the "complete" systems are described at two different MO levels. This method has been widely tested on several examples, including conformational analysis, geometry optimization, geometry and energy analysis of the stationary points, etc. The effects of the basis set, the method used in the low level of calculation, and the choice of the "model" system have been analyzed in detail. Humbel and co-workers[30] concluded that the IMOMO method produces results very similar to those of the full higher-level calculation for the "complete" system, and that the most important aspect of the method is its computational advantage.

To add flexibility to the geometry optimization in the previous methods taking into account the "link" atom, Corchado and Truhlar[37,38] proposed the integrated molecular orbital with harmonic cap (IMOHC) method, which includes an additive harmonic term in the original integrated method and allows the calculation of gradients, harmonic vibrational frequencies, and geometry optimization. It is interesting to note that in the limit of infinitely large values for the harmonic constant, the IMOHC method becomes equivalent to one possible way to implement the original IMOMO method. Thus, the original IMOMO method can be regarded as a particular case of the IMOHC method.[37] The IMOHC method, however, has the disadvantage of increasing the computational cost of the geometry optimization. Thus, for a system with N atoms and N_L link atoms, there will be $3N_L$ additional coordinates to be optimized with respect to the number of coordinates to be optimized in the original IMOMO scheme. Recently, we have studied[40] the performance of the IMOMO and IMOHC integrated methods in predicting geometry, harmonic vibrational frequencies, and energy changes (reaction energy and barrier height), using seven hydrogen abstraction reactions as test set. We concluded that, in general, the two integrated methods behave similarly, and that the success of these methods is mainly due to the higher-level "model" system description, the effect of the remaining lower-level fragments being smaller.

Comparatively, however, far less effort has been devoted to the study of the performance of the integrated methods in describing saddle points[30,40−45] and reaction paths.[41−45] Recently, our group developed and tested a new integrated method computational approach (RAIL, rate constant calculation with integrated levels)[45] to calculate the intrinsic reaction path (IRC), and thence to obtain kinetic and dynamic information for reactions involving the breaking−forming of covalent bonds in large molecules. Specifically, in that paper we used the IMOHC approach. We concluded that the new scheme reproduces the behavior of a benchmark calculation for such kinetic and dynamic properties as the minimum energy path (MEP) and ground-state vibrationally adiabatic potential curves, the localization of the bottleneck on the reaction path, and the non-Arrhenius behavior of the thermal rate constants with the tunneling effect. Moreover, the new scheme showed little dependency on which "low-level" was used in the computation. Basically, the RAIL method follows the "direct dynamics" approach using integrated levels to obtain the electronic information. However, the use of IMOHC represents RAIL's main disadvantage, since the computational cost increases due to the "link" atom optimization.

In the present work we study the CF_3CH_3 (HFC-143a) + OH system as a model of a hydrogen abstraction reaction. This reaction presents several important features that invite theoretical study. First, the knowledge of the kinetics of fluorocarbons (HFCs) with the hydroxyl radical, a replacement for the Earth's ozone layer destroying CFCs (chlorofluorocarbons), is very important for understanding their role in atmospheric processes, especially in the chemistry of stratospheric ozone. Second, it is a polyatomic reaction with six heavy atoms, which is hard to describe by ab initio calculations. And third, since it presents the heavy−light−heavy mass combination, it is a good candidate to present a large tunneling effect at low temperatures.[46,47]

Experimentally, there have been only a few studies of this reaction,[48−52] and then only over a small temperature range (260−425 K). The good agreement observed between the three last experiments lends confidence to the recommended Arrhenius expression,[53] $k(T) = 1.8 \times 10^{-12} \exp(-4312 \pm 300\text{-}(\text{calmol}^{-1})/RT)$ cm^3 molecule^{-1} s^{-1}. No curvature was found in the experimental and recommended Arrhenius plots. However, since the heavy−light−heavy mass combination is present in this reaction, curvature of the Arrhenius plot is expected. This disagreement concerning the curvature of the Arrhenius plot is probably simply a result of the small temperature range studied experimentally (260−425 K), and this effect should become more evident when a larger range of temperatures is analyzed.

This experimental work contrasts with the paucity of theoretical studies, due probably to the difficulty in describing the electronic structure of this large system. Studies have been limited to rate constant calculations using the conventional transition-state theory (TST). Jeong and Kaufman[54] carried out calculations using TST and estimated the tunneling factors by the Wigner and Eckart methods, which are known to underestimate this effect. Cohen and Benson[55] also used TST but did not include the tunneling effect in the calculation.

In the present paper, as a main goal we shall extend the idea of the integrated methods to the reaction-path construction in a chemical reaction, and thence to studying the kinetics and dynamics. We shall use the IMOMO approach for the first objective, and the variational transition-state theory (VTST) to obtain thermal rate constants and tunneling effects.

2. Methods and Computational Details

2.1. Electronic Structure Calculations. Geometry, energy, and first and second energy derivatives of all stationary points were calculated using the IMOMO method[27−33,39] implemented in the GAUSSIAN 98 program.[56] This method has been explained elsewhere, but for the sake of clarity and completeness, the most important features will be summarized here.

Let us write our reaction in an expanded form

$$CF_3CH_3 + OH \rightarrow [CF_3CH_2\cdots H\cdots OH]^{\ddagger} \rightarrow CF_3CH_2 + H_2O$$

where the reaction of methane with the hydroxyl radical is our "model" reaction

$$CH_4 + OH \rightarrow [CH_3\cdots H\cdots OH]^{\ddagger} \rightarrow CH_3 + H_2O$$

The "complete", "real", system (CS), $CF_3CH_3 + OH$, is formally divided into two parts, which are calculated at different levels of MO theory:

(i) The "model" system (MS), or inner layer, is the most active site of the reaction. Here the breaking−forming bonds are produced, in this case $-CH_2\cdots H\cdots OH$. Note that it is necessary to add a "link" atom onto the CH_2 fragment to ensure a saturated valence structure. This MS is calculated at the highest MO level (HL) possible and is denoted (MS, HL).

(ii) The rest of the system, or outer layer, F_3C- in this case, is calculated at a lower MO level (LL) and is denoted (CS, LL). Note that this case corresponds to the two-layer ONIOM method.[39]

The final integrated IMOMO method is then denoted (MS, HL):(CS, LL).

From a practical point of view, the energy of the "complete" system is approximated by

$$E_{CS}(I) = E_{CS}(LL) - E_{MS}(LL) + E_{MS}(HL) \quad (1)$$

where (I) denotes integrated level. Stated in this way, eq 1 considers the integrated calculation as the inclusion of higher-level effects in a lower-level calculation for the "complete" system.[37] Once the integrated energy has been defined, the corresponding gradient and Hessian expressions are

$$\nabla\mathbf{E}_{CS}(I) = \nabla\mathbf{E}_{CS}(LL) - \nabla\mathbf{E}_{MS}(LL)^*\mathbf{J}(r_2;r_1,r_3) + \nabla\mathbf{E}_{MS}(HL)^*\mathbf{J}(r_2;r_1,r_3) \quad (2)$$

and

$$\mathbf{H}_{CS}(I) = \mathbf{H}_{CS}(LL) - \mathbf{J}^T(r_2;r_1,r_3)^*\mathbf{H}_{MS}(LL)^*\mathbf{J}(r_2;r_1,r_3) + \mathbf{J}^T(r_2;r_1,r_3)^*\mathbf{H}_{MS}(HL)^*\mathbf{J}(r_2;r_1,r_3) \quad (3)$$

where $\mathbf{J}$ is the Jacobian matrix that projects the forces on all the set of "link" atoms (r_2) onto the common set of atoms in the "model" system and the "complete" system (r_1), and the set of atoms belonging to the "complete" system (r_3), and $\mathbf{J}^T$ is the transposed matrix (see the original paper[39] for computational details).

Once the geometry has been optimized, the harmonic vibrational frequencies are calculated from the integrated Hessian, $\mathbf{H}_{CS}(I)$. Finally, the diagonalization of the projected Hessian matrix provides us with $3N - 6$ vibrational frequencies, which are checked to be real frequencies in the reactants and products, while the saddle point was identified with one negative eigenvalue of the Hessian matrix and, therefore, one imaginary frequency.

In this paper, for the geometry optimization and frequency calculation, the MP2=FULL/6-31G(d,p) level (second-order Møller−Plesset perturbation theory with full electron correlation) was chosen as HL, while the HF/6-31G level (Hartree−Fock) was selected as LL. The choice of this low level is justified by the conclusions from earlier papers[35,40,45] that the integrated scheme shows little dependency on which "low level" is used. The integrated level is then denoted

MP2=FULL/6-31G(d,p):HF/6-31G

where the double point (X_1:X_2) denotes the integrated level used: X_1 is the higher level for the "model" system, and X_2 is the lower level for the "complete" system. This level is denoted Level 0.

In a second step, to improve the energy description of the stationary points, we made a single-point calculation at higher levels, i.e., calculation of the energy at a higher integrated level using the geometry optimized in the previous step:

Level I. Using the geometries optimized at Level 0, we made a single-point calculation with a better description of the "model" system using the CCSD(T)[57] (coupled-cluster approach with single and double substitutions including a perturbative estimate of connected triple substitutions) with the 6-311++G-(2df,p) basis set. We denote this energy as

CCSD(T)/6-311++G(2df,p):HF/6-31G//MP2= FULL/6-31G(d,p):HF/6-31G

where the double slash (X//Y) denotes geometry optimization at the level Y and energy calculated at level X, both integrated levels.

Level II. Continuing with the CCSD(T) approach, we used an enlarged basis set, namely, the correlation-consistent polarized valence triple-ζ developed by Dunning and co-workers (cc-pVTZ).[58] We denote this integrated energy as

CCSD(T)/cc-pVTZ:HF/6-31G//MP2= FULL/6-31G(d,p):HF/6-31G

Level III. We made a single-point calculation using the density functional theory, treating the exchange and correlation by the B3LYP protocol,[59] which is based on Beckes's three-parameter hybrid method (B3)[60] for combining Hartree−Fock exchange with a local density approximation exchange-correlation functional (LYP).[61] We use the same basis set as in Level I. It is well-known that this last method is a powerful and economic alternative in the description of large compounds, so that we can use these results for comparison with the integrated levels. We denote this energy as

B3LYP/6-311++G(2df,p)//MP2= FULL/6-31G(d,p):HF/6-31G

Note that the left-hand term in the double slash is a nonintegrated level.

2.2. Dynamics Calculations. At the MP2=FULL/6-31G(d,p):HF/6-31G integrated Level 0 we constructed the "intrinsic reaction coordinate" (IRC), or minimum energy path (MEP) starting from the saddle-point geometry and going downhill to both the asymptotic reactant and product channels in mass-weighted Cartesian coordinates with a gradient step size of 0.02 bohr amu$^{1/2}$. The Hessian matrix was evaluated at every point along the reaction path, always avoiding the undesirable reorientations of molecular geometries. Along this MEP the reaction coordinate, s, is defined as the signed distance from the saddle point, with $s > 0$ referring to the product side. In the rest of the work the units of s are bohr, and the reduced mass to scale the coordinates[62] is set to 1 amu. This has no effect on calculated observables, but it does affect the magnitude of 5 in plots used for interpretative purposes.

Along the MEP, we performed a generalized normal-mode analysis projecting out frequencies at each point along the path.[63] With this information, we first calculated the ground-state vibrationally adiabatic potential curve

$$V_a^G(s) = V_{MEP}(s) + \epsilon_{int}^G(s) \quad (4)$$

where $V_{MEP}(s)$ is the classical energy along the MEP with its zero energy at the reactants ($s = -\infty$) and $\epsilon_{int}^G(s)$ is the zero-point energy at s from the generalized normal-mode vibrations

orthogonal to the reaction coordinate. Second, we calculated the coupling terms,[63,64,65] $B_{k,F}(s)$, measuring the coupling between the normal mode k and the motion along the reaction coordinate, mode F. These coupling terms are the components of the reaction-path curvature, $\kappa(s)$, defined as

$$\kappa(s) = (\sum [B_{k,F}(s)]^2)^{1/2} \qquad (5)$$

and they control the nonadiabatic flow of energy between these modes and the reaction coordinate.[63,64,65] These coupling terms will allow us to calculate accurate semiclassical tunneling factors, and to give a qualitative explanation of the possible vibrational excitation of reactants and/or products, i.e., dynamical features.

Finally, the energies, vibrational frequencies, geometries and gradients along the MEP were used to estimate rate constants by using variational transition-state theory (VTST). We calculated thermal rates using the canonical variational theory[46,66] (CVT) approach, which locates the dividing surface between reactants and products at a point $s^{*CVT}(T)$ along the reaction path that minimizes the generalized TST rate constants, $k^{GT}(T,s)$ for a given temperature T. Thermodynamically, this is equivalent to locating the transition state at the maximum $\Delta G^{GT,o}[T,s^{*CVT}(T)]$ of the free energy of activation profile $\Delta G(T,s)$.[46,66] Thus, the thermal rate constant will be given by

$$k^{CVT}(T) = \sigma \frac{k_B T}{h} K^o \exp[-\Delta G(T,s^{*CVT})/k_B T] \qquad (6)$$

with k_B being Boltzmann's constant, h Planck's constant, σ the symmetry factor (the number of equivalent reaction paths, which were assumed to be 3 and 2 for the forward and reverse reactions, respectively), and K^o the reciprocal of the standard-state concentration, taken as 1 molecule cm^{-3}.

In the present work, we used the general polyatomic rate constants code GAUSSRATE,[67] which is an implementation based on the GAUSSIAN 98[56] and the POLYRATE.[68] programs. Note that the current version of GAUSSRATE is based on the GAUSSIAN 94 program, which does not implement the IMOMO approach. In the present work some subroutines have been modified in order to run the GAUSSIAN 98 program, which does include the IMOMO approach. Since integrated methods are used, this version of GAUSSRATE is equivalent to our RAIL method. The rotational partition functions were calculated classically. The vibrational mode associated with the free rotation of the OH fragment at the saddle point and along the MEP is treated using the hindered rotor model,[69] and all other vibrational modes are treated as quantum-mechanical separable harmonic oscillators, with the generalized normal-modes defined in redundant curvilinear coordinates.[70,71] The curvilinear coordinates chosen were all the possible bond lengths and angles. The advantage of curvilinear coordinates (nonlinear functions of Cartesian coordinates) over rectilinear ones (linear functions of Cartesian coordinates) is that in some cases the lowest bending frequencies have unphysical imaginary values over a wide range of the reaction coordinate using rectilinear coordinates, whereas these frequencies are real over the whole of the reaction path using curvilinear coordinates. This behavior has been verified in the title reaction and other hydrogen abstraction reactions.[72−74] In calculating electronic partition functions, we included the two electronic states for the OH reactant, with a 140 cm^{-1} splitting. We also considered the tunneling contribution. As we have information only on the reaction path, centrifugal-dominant small-curvature tunneling (SCT)[75] was used. Methods for large curvature cases have been developed,[76] but they require more information about the PES than was determined in the present study.

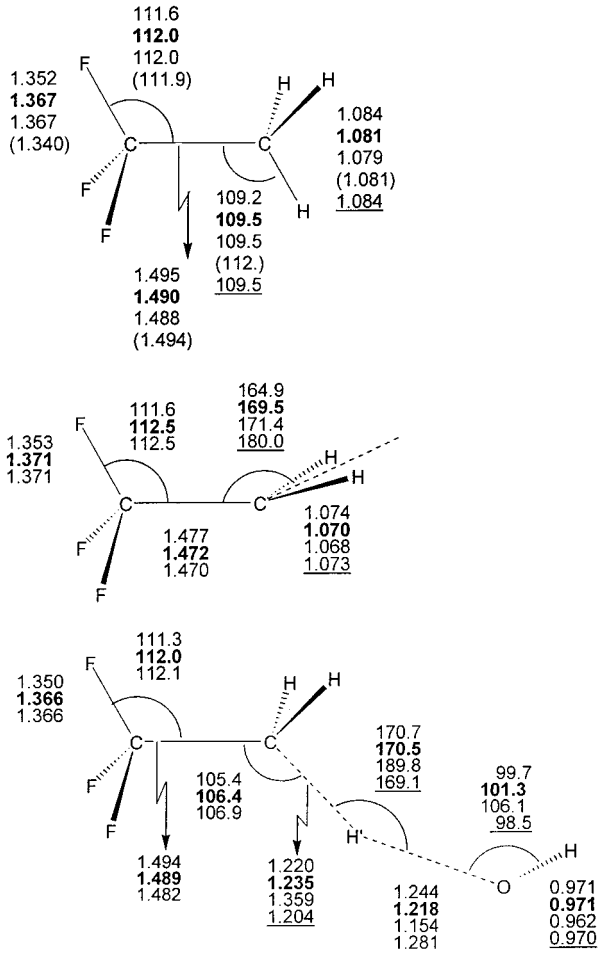

Figure 1. Optimized stationary point geometries at several levels: first entry, MP2=FULL/6-31G(d,p); second entry, integrated MP2:HF (bold); third entry, HF/6-31G; fourth entry, experimental values (in parentheses); fifth entry, MP2=FULL/6-31G(d,p) level for the "model" system, CH_4 + OH (underlined).

3. Results and Discussion

3.1. Structures and Vibrational Frequencies. The optimized geometries of reactant (CF_3CH_3), product (CF_3CH_2) and saddle point, using the IMOMO [MP2=FULL/6-31G(d,p):HF/6-31G] method are shown in Figure 1, and the corresponding harmonic vibrational frequencies are listed in Table 1. The values for the low-level (HF/6-31G) and the high-level [MP2=FULL/6-31G-(d,p)] single levels for all stationary points are also included for comparison.

Taking into account that in the IMOMO approach the "complete" system is divided into two parts, which are described at different MO levels, we can distinguish between the parameters (bonds, angle and normal modes) of the "model" system and the parameters of the "rest" of the system. The IMOMO parameters (Figure 1 and Table 1) agree with the high-level values for those parameters belonging to the "model" system (R_{C-H}, $R_{C-H'}$, $R_{H'-O}$, R_{O-H}, $\angle CH'O$, $\angle H'OH$), with the low-level values for the parameters that belong to the "rest" of the system (R_{C-F}, $\angle FCF$), and they are intermediate between the two parts (R_{C-C}, $\angle CCH$, ZPEs). This is the behavior expected for integrated methods.[39,40]

With respect to the experimental geometry of 1,1,1-trifluoroethane,[77] the only values available for comparison, the high-

TABLE 1: Harmonic Vibrational Frequencies (cm^{-1}) and Zero-Point Energy (ZPE, in kcal mol^{-1}) for the Stationary Points at Several Calculation Levels

CF_3CH_3			CF_3CH_2			SP		
MP2[a]	IMOMO[b]	HF[c]	MP2[a]	IMOMO[b]	HF[c]	MP2[a]	IMOMO[b]	HF[c]
3282	3324 (3283)[d]	3337	3436	3483 (3440)[e]	3497	3830	3825 (3845)[f]	3910
3282	3324 (3283)	3337	3301	3343 (3440)	3362	3318	3360 (3322)	3411
3169	3207 (3283)	3244		(3243)		3219	3258 (3318)	3311
	(3135)						(3177)	
1548	1552 (1627)	1636	1525	1550 (1491)	1591	1524	1536 (1545)	1634
1548	1552 (1627)	1636	1358	1422 (1491)	1432	1517	1518 (1521)	1602
1496	1520 (1406)	1610	1300	1383	1391	1367	1422 (1465)	1430
1342	1409 (1406)	1427	1211	1268	1269	1328	1383 (1327)	1403
1308	1371 (1406)	1400	975	1036	1053	1290	1333	1335
1308	1371	1400	873	889	891	1245	1231 (1207)	
	1243							
1018	1064	1099	623	630	645	1084	1095	1121
1018	1064	1099	610	620	623	1000	1035 (940)	1061
851	864	866	535	545	547	906	894	895
605	610	611	504	504	518	837	826	818
539	546	549	376	392 (395)	394	735	728 (744)	627
539	546	549	342	356	366	604	613	604
368	376	380	151	117	106	537	545	547
368	376	380				528	539	527
261	246	247				401	406	447
						356	361 (356)	370
						317	338 (292)	328
						185	215	182
						100	101	98
						58	65 (31)	60
						2279i	1823i (2060i)	3250i

[a] Single level: MP2=FULL/6-31G(d,p). [b] Integrated Level 0: MP2=FULL/6-31G(d,p):HF/6-31G. [c] Single level: HF/6-31G. [d] Values for CH_4 at the higher level are given in parentheses. [e] Values for CH_3 at the higher level are given in parentheses. [f] Values for CH_4+OH saddle point at the higher level are given in parentheses.

level MP2 and the IMOMO methods lead to agreement, while the low-level HF is not even close. In the case of the product, a very sensitive test is the pyramidalization of the radical center (Figure 1). The IMOMO value is intermediate between the high and the low levels, with an angle of 169.5°. The pyramidalization of the radical contrasts with the planar structure of the methyl radical (the "model" system) and has also been found with other substituents.[40,78,79]

For the saddle point, the most sensitive parameters are related to the breaking−forming bonds, C−H′, H′−O and ∠C−H′−O. At the IMOMO level, the length of the bond that is broken (C−H′) increases by only 14%, while the length of the bond that is formed (H′−O) increases by 27% with respect to the reactant (CF_3CH_3) and product (H_2O) molecules, respectively. Therefore, the reaction of the CF_3CH_3 with the hydroxyl radical proceeds via an "early" transition state. This is the expected behavior that would follow from Hammond's postulate,[80] since that reaction is exothermic (see Table 2). This saddle point was identified with one negative eigenvalue of the Hessian matrix and, therefore, one imaginary frequency (1823i cm^{-1}). Furthermore, the OH fragment is not in the CCH′O plane but is displaced by 34.5°.

3.2. Energy Properties. Table 2 lists the energy and enthalpy (0 K) changes relative to the reactants at several single and integrated levels. We begin by analyzing the heat of reaction because a comparison with experiment is possible, which will enable us to estimate the accuracy of the levels used. The experimental enthalpy of reaction has not been directly measured. It was obtained here from the corresponding standard enthalpies of formation (298 K) and then corrected to 0 K:

$$\Delta H_R(298\ \mathrm{K}) = \sum k_i(\Delta H^\circ_f)_i(298\ \mathrm{K})$$

where the thermal corrections were calculated with standard methods of statitistical thermodynamics using information from the optimized geometries at Level 0.

TABLE 2: Energy and Enthalpy (0 K) Changes Relative to Reactants (kcal mol^{-1}) at Several Levels

level	R	SP	P
		ΔE	
HF[a]	0.0	33.81	+8.83
MP2[b]		13.56	−8.27
Level 0[c]		11.57	−8.41
Level I[d]		10.02	−9.37
Level II[e]		9.69	−9.39
Level III[f]		5.14	−11.24
model reaction[g]	0.0	12.06	−9.88
		ΔH(0 K)	
HF	0.0	31.42	+7.29
MP2		11.20	−9.65
Level 0		9.37	−9.87
Level I		7.82	−10.83
		7.49	−10.85
Level III		2.94	−12.70
exp[h]			−12.2 ± 3.2
model reaction	0.0	10.34	−11.58

[a] Single level: HF/6-31G. [b] Single level: MP2=FULL/6-31G(d,p). [c] Integrated Level 0: MP2=FULL/6-31G(d,p):HF/6-31G. [d] Integrated level: CCSD(T)/6-311++G(2df,p):HF/6-31G//Level 0. [e] Integrated level: CCSD(T)/cc-pVTZ:HF/6-31G//Level 0. [f] Single level: B3LYP/6-311++G(2df,p)//Level 0. [g] CH_4 + OH → CH_3 + H_2O at the MP2=FULL/6-31G(d,p) single level. [h] $\Delta H_R(0\ \mathrm{K}) = \Delta H_R(298\ \mathrm{K})$ − thermal corrections (298 → 0) = $\sum k_i(\Delta H^\circ_f)_i$ − thermal corrections (298 → 0).

However, for this reaction this magnitude presents a problem that has to be addressed separately. While the enthalpies of formation of OH (9.3 kcal mol^{-1}) and H_2O (−57.81 kcal mol^{-1}) have been established satisfactorily experimentally,[53] the CF_3-CH_3 molecule and the CF_3CH_2 radical have been less well studied experimentally. The JPL report[53] recommends a value

TABLE 3: Barrier Height (kcal mol^{-1}) for the CH_4 + OH → CH_3 + H_2O Model Reaction at Several Very High ab Initio Levels

method	$\Delta E^{\neq}$	$\Delta H^{\neq}$(0 K)	ref
CBS/QCI/APNO	5.11		84
G2		5.9	85
G2M	5.3		86
MP2/cc-pVTZ	8.38	7.01	87
MP2/aug-cc-pVTZ	7.96	6.48	87
CCSD(T)/6-311++G(2df,2p)	7.45		20
CCSD(T)/cc-pVTZ	7.08	5.71	87
CCSD(T)/aug-cc-pVTZ	5.83	4.46	85
CCSD(T)-SAC/cc-pVTZ	4.97	3.60	87

of -179 ± 2 kcal mol^{-1} for the former, and Wu and Rodgers[81] obtained a value of -123.6 ± 1.2 kcal mol^{-1} for the radical from equilibrium constants determined spectroscopically. With this information, the enthalpy of reaction (298 K) is -11.7 ± 3.2 kcal mol^{-1} [$\Delta H_R(0\ K) = -12.2 \pm 3.2$ kcal mol^{-1}]. This wide margin of error makes the direct comparison of theory/experiment difficult.

With these considerations in mind, we shall now analyze our theoretical results. While the reaction is experimentally exothermic, the HF single-level calculation yields an endothermic reaction. The inclusion of some correlation at the MP2 single-level already yields the correct sign and a value within the error limits. Interestingly, the integrated Level 0 yields similar results, but with a lower computational cost. A closer agreement with experiment is obtained when more correlation energy and larger basis sets are considered (Levels I−III), althougth it is well-known[82,83] that the CCSD(T) level has a tendency to underestimate the reaction energies of hydrogen abstraction reactions due to the slow convergence of the calculations with the dimensions of the basis sets. However, it is worth mentioning that this is a general problem in computational chemistry and is not due to the nature of the integrated method used.

With respect to the barrier height a direct comparison with experiment is not possible. The HF single-level and Level III, which uses the B3LYP method, markedly overestimate and underestimate, respectively, the barrier height. As was noted in the Introduction, this behavior of the B3LYP level is common to the DFT and hybrid DFT methods for hydrogen abstraction reactions[12−20] and argues against their use in kinetics and dynamics studies. As in the enthalpy of reaction case, Level 0 reproduces the values of the MP2 single level at a lower computational cost. Therefore, the IMOMO scheme appears to be a successful and promising computational tool to overcome one of the main drawbacks of the DFT and hybrid DFT methods. Moreover, it shows its effectiveness in correcting wrong potential energy surfaces at a low computational cost.

When we raise the calculation level (Level 0 → Level II) the barrier height is lowered by several kcal mol^{-1}, and it may be expected that a more accurate barrier height would be obtained using highly correlated wave functions and larger basis sets, which is beyond of our computational capacity. To obtain an estimate of our limitations, we analyzed the "model" reaction CH_4 + OH, which has been extensively studied at very high levels. Table 3 lists the more recent results.[20,84−87] When highly correlated wave functions and large basis sets are used (in some cases in combination with extrapolated approaches), the barrier height ranges from 4.97 to 5.83 kcal mol^{-1}, i.e., $\approx 1-2$ kcal mol^{-1} lower than the CCSD(T)/cc-pVTZ result, which is equivalent to our highest level used, Level II. The exceptions are Lynch and Truhlar's result,[20] which yields a value of 7.45 kcal mol^{-1} (see Table 3), and Lynch and Truhlar's estimation[20,88] of the true barrier height, based on analyzing experiments, which is slightly higher, 6.7 kcal mol^{-1}. Interestingly, the error in the energy reaction is equivalent to our error estimate of the barrier height. Therefore, from these comparisons we estimate that the barrier height for the "complete" system using integrated methods will be overestimated, at least, by this same amount (upper limit). Masgrau and co-workers[87] pessimistically stated that even though they used the highest ab initio electronic level reported up to now for dynamics calculations of the CH_4 + OH reaction, the experimental rate constants were not exactly matched. Clearly, this situation will become worse in the case of larger systems, such as the title reaction.

3.3. The "Model" Reaction. To understand the influence of the description of the "model" reaction, CH_4 + OH → CH_3 + H_2O, on the geometry, vibrational frequency and energies of the IMOMO method, Figure 1, Table 1, and Table 2 also show these magnitudes for the "model" reaction at the high-level MP2=FULL/6-31G(d,p).

First, the geometries of the reactant and the product agree with the "model" part (inner layer) of the IMOMO method, with the exception of the pyramidalization of the CH_3 radical, which was explained above. The broken and formed bonds and the angle of the saddle point in the "model" reaction reproduce the behavior of the "complete" system. Thus, the bond that is broken (C−H′) increases by only 11% and the length of the bond that is formed (H′−O) increases by 33%. This transition state is "earlier" than its homologue in the "complete" system, which is consistent with the greater exothermicity of the "model" reaction at the common level, MP2.

Second, the common frequencies in the "model" reaction (values in parentheses in Table 1) and the "complete" system are in reasonable agreement, and the lowest frequencies, which appear in the "complete" system but not in the "model" reaction, are values very close to those calculated at the low level, as was expected. The imaginary frequency, 2060i cm^{-1}, at the saddle point is close to the value in the "complete" system.

Third, the "model" reaction simulates the energy and enthalpy (0 K) changes (reaction and activation) of the "complete" system at the common level, MP2.

Therefore, in light of this comparison, it seems that the success of the IMOMO approach is mainly due to the HL "model" system description, and the effects of the remaining LL fragments is smaller. This conclusion agrees with earlier studies by our group[45] using the IMOHC approach.

3.4. Possibility of Intermediate Complexes. For the title reaction, CF_3CH_3 + OH, a priori the reaction of the hydroxyl radical with the CF_3CH_3 molecule would proceed via a reactant complex (CF_3CH_2−H···OH, denoted RC) in the entrance channel, and a product complex (CF_3CH_2···H−OH, denoted PC) in the exit channel.

The two complexes, RC and PC, were theoretically searched for in this work at Level 0 in two independent ways. On one hand, we followed the conventional method of approaching the two subsystems from infinity; and, on the other hand, we followed the IRC starting from the saddle point and going downhill to both reactant and product channels. All the attempts with this integrated method, Level 0, proved unsuccessful, either by computational problems, i.e., SCF energy convergence could not be achieved, or by conceptual problems, i.e., a true minimum (zero imaginary frequencies) could not be obtained. In summary, we conclude that at this integrated level the reaction CF_3CH_3 + OH proceeds as a direct hydrogen abstraction reaction without intermediate complexes.

This result is not surprising and it agrees with the theoretical studies for the CH_4 + OH "model" reaction.[87,89,90] Basch and

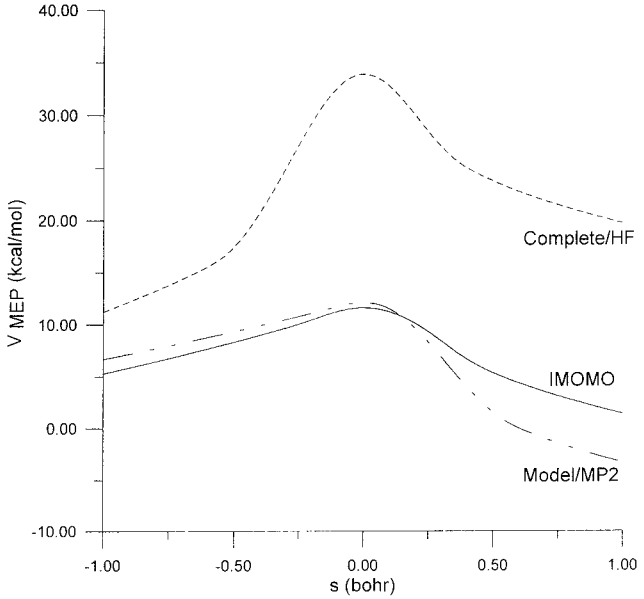

Figure 2. Classical potential energy curves (V_{MEP}) with respect to the reactants as a function of *s*, for complete/HF (dashed line), IMOMO (solid line), and model/MP2 (solid-dashed line).

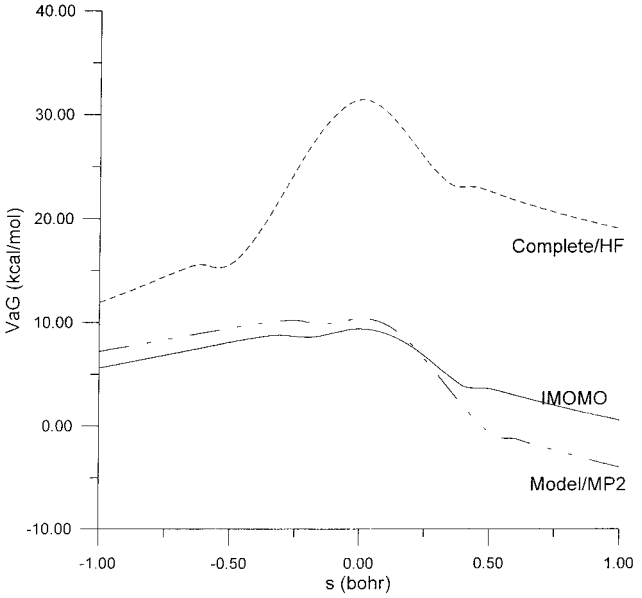

Figure 3. Vibrationally adiabatic potential energy curves (ΔV_a^G) with respect to the reactants as a function of *s*, for complete/HF (dashed line), IMOMO (solid line), and model/MP2 (solid-dashed line). Rectilinear coordinates are used for comparison.

Hoz[89] using ab initio calculations found a complex in the entrance channel that does not have the expected $CH_3-H\cdots OH$ geometry and is not on the IRC. Instead the $CH_4\cdots HO$ geometry is preferred. More recently, Wheeler and co-workers[90] have found experimentally a similar complex in the entrance channel. In the exit channel, Basch and Hoz find a complex $CH_3\cdots HOH$ that is so weak that it is not stable energetically after inclusion of the ZPE; i.e., this complex does not support any bound vibrational level. In Masgrau and co-workers[87] recent higher-level ab initio calculations, they also find the product complex but in this case it is weakly bound at 0 K and higher temperatures.

3.5. Reaction-Path Analysis. Having analyzed the stationary points, we now extend the IMOMO scheme to construct the reaction path. The analysis of the reaction path is carried out on the information (energy, gradient, and Hessian) at the integrated Level 0 [MP2=FULL/6-31G(d,p):HF/6-31G] over the *s* range −2.0 to +2.0 bohr. For comparison purposes, we also constructed the reaction path at the single lower-level HF/6-31G, and for the "model" reaction, $CH_4 + OH$, at the single higher-level MP2=FULL/6-31G(d,p), in these cases, over the *s* range −1.0 to +1.0 bohr.

We begin by comparing these three cases. The classical energy along the MEP, V_{MEP}, the ground-state vibrationally adiabatic potential energy, ΔV_a^G, and the change in the local zero-point energy, ΔZPE, curves as a function of *s* over the common range are shown in Figures 2−4, respectively. Note that ΔV_a^G and ΔZPE are defined as the difference between these magnitudes at *s* and their values for the reactants. In all three cases, the complete/HF low level is very far from the IMOMO results, indicating that it is not adequate for representing the potential energy surface. Again, the "model" reaction reproduces the energy, V_{MEP}, enthalpy at 0 K, ΔV_a^G, and zero-point energy change, ΔZPE, of the "complete" system at the same level, indicating that the success of the integrated approach is mainly due to the high-level "model" system description.

We now analyze the "complete" system at Level 0. Figure 5 shows the V_{MEP}, the ΔV_a^G, and the ΔZPE, as a function of *s*, and Figure 6 shows some vibrational frequencies along the MEP. The behavior is that expected in hydrogen abstraction reactions,

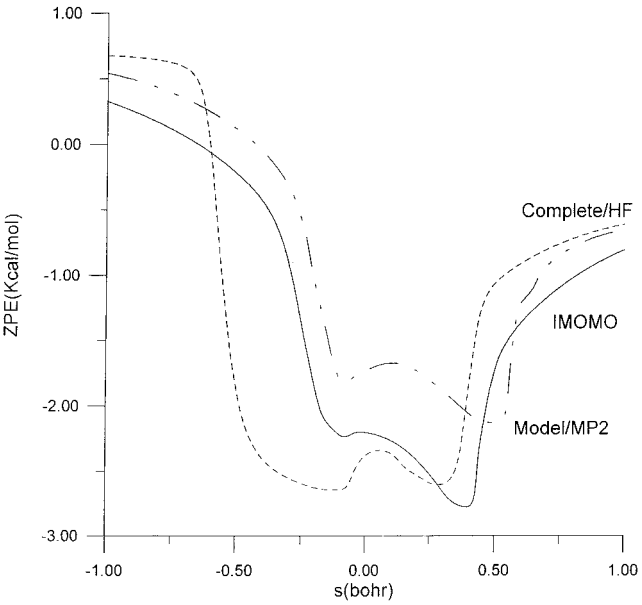

Figure 4. Zero-point energy curves (ΔZPE) with respect to the reactants as a function of *s*, for complete/HF (dashed line), IMOMO (solid line), and model/MP2 (solid-dashed line). Rectilinear coordinates are used for comparison.

thus indicating the success of the integrated approach in the description of this type of reaction. The mode related to the breaking (C−H′)−forming (H′−O) bonds drops dramatically near the saddle point (*reactive mode*). This mode presents a widening of the vibrational well, an effect that has been found in other reactions with a small skew angle.[47,91,92] The lowest vibrational frequencies along the reaction path (*transitional modes*) correspond to the transformation of free rotations or free translations of the reactant limit into real vibrational motions in the overall system. Their frequencies tend asymptotically to zero at the reactant and product limits and reach their maximum in the saddle-point zone. Therefore, in the sadde-point region, the behavior of these transitional modes only partially com-

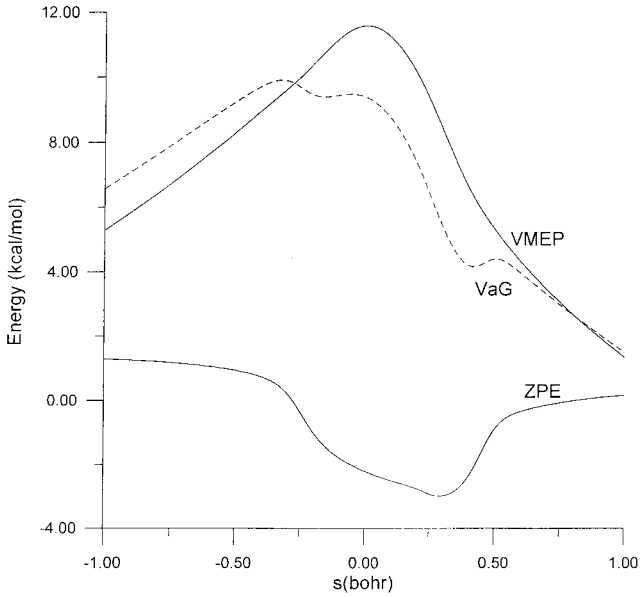

Figure 5. Classical potential energy (V_{MEP}), vibrationally adiabatic potential energy (ΔV_a^G), and zero-point energy (ΔZPE) curves with respect to the reactants as a function of *s* for the "complete" system at the IMOMO level, and using curvilinear coordinates.

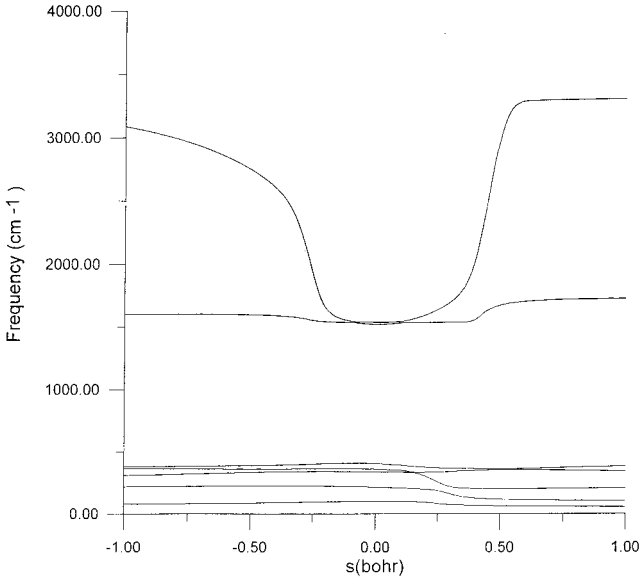

Figure 6. Some generalized normal-mode vibrational frequencies plotted versus *s*.

pensates the fall in the ZPE caused by the reactive mode, and as a result the ZPE shows noticeable changes with *s* (Figure 5).

Further analyzing the reaction valley, the curvature term (κ) of the reaction path as a function of *s* is plotted in Figure 7, which permits us to give a qualitative analysis of the vibrational excitation of reactants and products. There are two peaks, one on the reactant side, which has a value of 4.99 au at $s = -0.28$ bohr, and one on the product side of the saddle point, which has a value of 5.84 au at $s = +0.48$ bohr. The former is due to strong coupling of the reaction path to the CH′ reactive stretching ($B_{kF} = 4.63$ au) and a combination of bending ∠HCH, ∠CCH and stretching C−C ($B_{kF} = 0.97$ au) modes. Excitation of these modes might be expected to enhance the forward reaction rates. The second peak is in the exit channel and is higher than the first. It is due to the coupling of the reaction path to the OH stretching ($B_{kF} = 5.65$ au) and the HOH bending

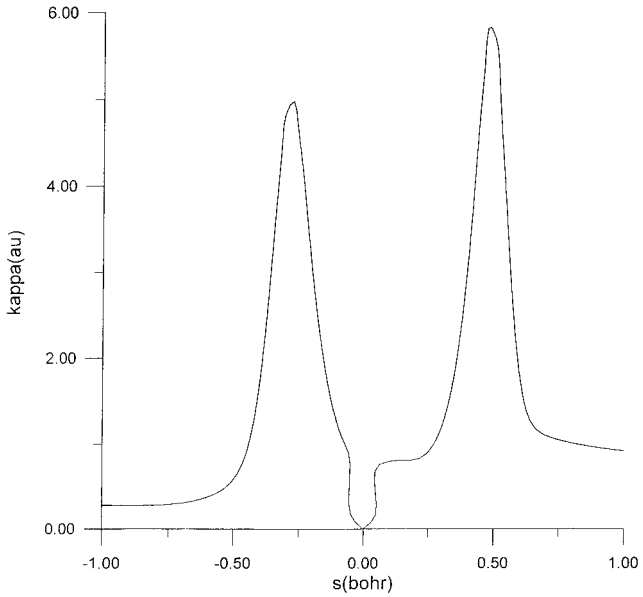

Figure 7. Curvature of the reaction path (κ factor) as a function of *s*.

($B_{kF} = 1.12$ au) modes. This is an indication that the OH stretching and the H_2O bending modes could appear vibrationally excited. Unfortunately, a comparison with experiment is not possible.

3.6. Improved Reaction Path. The poor energy description with the integrated Level 0 (see section 3.2 and Table 2) means that we have to optimize our integrated reaction path. In previous papers[91,93,94] we analyzed different approximations and found that the best choice was to scale the original curve (MP2:HF Level 0) regularly by a factor

$$F = \Delta E(\text{MP2:HF},s=0)/\Delta E(\text{Level II},s=0)$$

where ΔE is the variation of energy at each level with respect to the reactants. At the saddle point, $s = 0$, the barrier height is that of the highest level, Level II in this case. This factor is 0.837.

3.7. Rate Constants. In the canonical version of VTST, CVT, the dividing surface is varied along the reaction path to minimize the rate constants, obtaining the generalized transition state (GTS) at the value *s**. Thermodynamically, the minimum rate constant criterion is equivalent to maximizing the generalized standard-state free energy of activation, $\Delta G^{GT,o}(T,s)$, eq 6. Therefore, the effects of the potential energy, entropy and temperature on the location of this GTS must be considered. In the present case, the bottleneck properties of the reaction, based on the CVT approach, show that the location of the GTS is away from the saddle point: from −0.323 to −0.308 bohr over the temperature range 250−500 K. Thus the variational effects, i.e., the ratio between variational CVT and conventional TST rate constants, are important. This result agrees with the behavior of the "model" system, CH_4 + OH, which also presents large variational effects.[87,95,96]

In Table 4 the calculated conventional TST and variational CVT rate constants at the scaled Level 0 (factor 0.837, Level II reference, $\Delta E^{\ddagger} = 9.69$ kcal mol^{-1}) are compared to experimental values in the temperature range 250−500 K. First, the large difference between the TST and CVT rates confirms our conclusion about the variational effects. Second, the tunneling effect is important in this temperature range, and comparable to the results obtained with the "model" reaction, CH_4 + OH,[96] indicating again the importance of an adequate description of the "model" reaction. Finally, our theoretical

TABLE 4: Rate Constants for the CF_3CH_3 + OH Reaction[a]

	scaled[b]				fitted[c]	
T (K)	TST	CVT	SCT	CVT/SCT	CVT/SCT	exp[d]
250	1.93(−19)	3.48(−20)	12.20	4.25(−19)	2.83(−16)	3.10(−16)
300	2.56(−18)	6.15(−19)	5.72	3.50(−18)	9.57(−16)	1.30(−15)
350	2.00(−179	5.12(−18)	3.63	2.00(−17)	2.55(−15)	3.66(−15)
400	7.31(−17)	2.44(−17)	2.72	6.64(−17)	5.23(−15)	7.93(−15)
450	2.36(−16)	8.68(−17)	2.23	1.93(−16)	9.80(−15)	1.45(−14)
500	6.20(−16)	2.44(−16)	1.92	4.69(−16)	1.67(−14)	2.35(−14)

[a] 4.25(−19) stands for 4.25×10^{-19}, in cm^3 $molecule^{-1}$ s^{-1}. [b] Level 0*0.837, $\Delta E^{\ddagger} = 9.69$ kcal mol^{-1}. [c] Level 0*0.420, $\Delta E^{\ddagger} = 4.90$ kcal mol^{-1}. [d] Reference 53.

TABLE 5: Comparative Cost with Respect to the MP2 Level (100%)

	relative cost (%)	
method	time	memory
MP2[a]	100	100
HF	0.7	3.5
Level 0	0.9	6.9

[a] The real time and memory at this level are 9 h 30 min and 2.3 GB, respectively, for each Hessian calculation.

results strongly underestimate the experimental data, by factors of 10^3 to 10^2 in the temperature range 250−500 K. The problem arises from the use of an incomplete basis set, and from the partial introduction of correlation energy at the CCSD(T) level. At this point it is worth mentioning that this limitation is not due to the nature of the integrated approach, since this same problem is found for the "model" system using high ab initio electronic structure calculations.[87]

To match the experimental data, we have to continue lowering the barrier height, and a reasonable agreement is found when the barrier height is 4.90 kcal mol^{-1} (fitted-Level 0 values in Table 4). Interestingly, this value is close to the barrier height for the "model" reaction (see Table 3). The differences with the experimental values can be explained because only the small curvature tunneling effect is considered in this work, when really the system presents a large curvature effect.

In this small range of temperatures (250−500 K) our theoretical results show no curvature of the Arrhenius plot, in accordance with the experimental evidence. However, when a larger range of temperatures is analyzed (250−1500 K) the Arrhenius plot is curved, which is the expected behavior in a reaction with a heavy light-heavy mass combination (values not shown).

The activation energy can be obtained from total rate constants through the usual definition

$$E_a = -R\, \mathrm{d}(\ln k)/\mathrm{d}(1/T) \qquad (7)$$

which is equivalent to determining the slope of the Arrhenius plot. The values are 6.84 and 4.14 kcal mol^{-1} for the scaled- and fitted-Level 0 approaches, respectively, versus the experimental value,[53] 4.31 kcal mol^{-1}.

3.8. Computational Cost. Another important factor in choosing the computational method is the cost. To compare between the different methods, we shall use the computational cost (time and memory) of the Hessian matrix calculation at one point of the reaction path. Table 5 lists the percentage relative cost with respect to the MP2 single-level calculation. The integrated level presents a considerable savings in computational effort (time and memory) by a factor of 100 in time, and 15 in memory, and is only a little more expensive than the HF low level. This saving is more important in the case of chemical reactions because of the large number of calculations (energy, gradient, and Hessian) along the reaction path.

While this relative comparison in percentages is very interesting, it does not give the true sense of the computational savings. Thus, each Hessian calculation at the MP2 level needs 9 h 30 min and 2.3 GB of memory, while the integrated Level 0 (MP2:HF) needs only 20 min and 0.16 GB. The time and memory saving are clearly considerable, and it is to be expected that this advantage will increase when larger molecular systems are involved.

3.9. Tropospheric Lifetimes. The main removal process for HFCs in the troposphere is the reaction with hydroxyl radicals. Talukdar and co-workers[50] using one-dimensional photochemical model find a troposphere lifetime of 74 years, while Orkin and co-workers[52] with indirect measurements using methylchloroform as reference and the Prather and Spivakowsky atmospheric model[97] find a value of 51 years.

To estimate the lifetime in the troposphere, we used two approximations. In the simplest approximation,[98,99] the tropospheric residence time is given by

$$\tau_{HFC} = (k(CF_3CH_3{+}OH)[OH])^{-1} \qquad (8)$$

where $[OH] = 2 \times 10^6$ molecules cm^{-3}. With our rate constant calculated at 277 K, we obtained a lifetime of 28 years, below the experimental values. With the more sophisticated model of Prather and Spivakovsky[97] the lifetime of HFC-143a is given by

$$\tau_{HFC} = [k_{MC}(277)/k_{HFC}(277)]\tau_{MC} \qquad (9)$$

where $k_{MC}(277)$ and τ_{MC} are the rate constant at 277 K and the corrected lifetime (5.7 years) of the methylchloroform (MC) reference, respectively. With our rate constant at 277 K, we obtained a lifetime of 67 years, in agreement with the experimental values.

4. Conclusions

In this paper we have constructed the intrinsic reaction path, and thence kinetic and dynamic information, using the IMOMO approach. We chose the hydrogen abstraction reaction CF_3CH_3 + OH as an example of a large reactive system ("complete" system), using CH_4 + OH as the "model " system.

With respect to the stationary points, the analysis of the geometry and frequencies showed that the parameters localized in the "model " system or inner layer have the accuracy of the high level, those localized in the outer layer are similar to the low level, and those connecting the two layers are intermediate in behavior. This is especially interesting in the saddle-point description, where the breaking−forming zone is simulated with the "model " system, and therefore described with the accuracy of the high-level at a lower computational cost. The analysis of the energy and enthalpy (0 K) changes (reaction and activation) showed that the success of the integrated method is mainly due to the higher-level "model " system description, the effect of the remaining lower-level fragments being smaller. The barrier height strongly depends on the level of calculation and basis set, and, to obtain accurate values, highly correlated wave functions and very large basis sets are necessary, with the consequent increase in computational cost. Interestingly, this is a general problem of computational chemistry and is not related to the integrated method.

With respect to the reaction path, the IMOMO approach reproduces the shape of the MEP and V_a^G curves given by the "model " system at the higher level. First, the variation of the

ZPE shows noticeable changes along the reaction path, with a wide minimum in the saddle-point region, which causes fairly marked variational effects. Second, the C−H stretching mode strongly couples with the reaction coordinate in the entrance channel, and therefore vibrational excitation of this mode might be expected to enhance the forward reaction rates. In the exit channel, the stretching and bending modes of water couple with the reaction coordinate, and these modes could appear vibrationally excited. The behavior is that expected in hydrogen abstraction reactions, thus indicating the success of the integrated approach in describing this type of reactions.

To calculate the rate constants using the variational transition-state theory with multidimensional tunneling, the reaction path was scaled to higher levels of calculation using the single-point calculation technique. Even at high levels, our theoretical results strongly underestimate the experimental values, indicating that the problem arises from the use of incomplete basis sets and the only partial introduction of correlation energy, also a general problem in computational chemistry, and not directly related to the integrated method used.

In sum, the integrated method corrects the deficiencies of the lower-level method and shows its effectiveness in correcting wrong potential energy surfaces at a very low computational cost, which is especially interesting for the study of large molecules.

Acknowledgment. I am grateful to Prof. Donald G. Truhlar for providing a copy of the GAUSSRATE program, to Dr. José C. Corchado by the computational support, and to the Consejeria de Educación, Ciencia y Tecnología, Junta de Extremadura (Spain) (Projects No. IPR99-A009 and 2PR01A002) for partial support of this work

References and Notes

(1) Doubleday, C.; McIver, J. W.; Page, M. *J. Phys. Chem.* **1988**, 92, 4367.
(2) Baldridge, K. M.; Gordon, M. S.; Steckler, R.; Truhlar, D. G. *J. Phys. Chem.* **1989**, *93*, 5107.
(3) Truhlar, D. G.; Gordon, M. S. *Science* **1990**, *249*, 491.
(4) Parr, R. G.; Yang, W. *Density Functional Theory of Atoms and Molecules*; Oxford University Press: New York, 1989.
(5) Dreizler, R. M.; Gross, E. K. U. *Density Functional Theory*; Springer-Verlag: Berlin, 1990.
(6) Labanowski, J. K., Andzelm, J. E., Eds. *Density Functional Methods in Chemistry*; Springer-Verlag: Berlin, 1991.
(7) Bartolotti, L. J.; Flurchick, K. In *Reviews in Computational Chemistry*; Lipkowitz, K. B., Boyd, D. B., Eds.; VCH Publishers Inc.: Deerfield Beach, FL, 1996; Vol. 7, p 187.
(8) St. Amant, A. In *Reviews in Computational Chemistry*; Lipkowitz, K. B., Boyd, D. B., Eds.; VCH Publishers Inc.: Deerfield Beach, FL, 1996; Vol. 7, p 217.
(9) Ziegler, T. *Chem. Rev.* **1991**, *91*, 651.
(10) Bauslicher, C. W. *Chem. Phys. Lett.* **1995**, *246*, 40.
(11) Redfern, P. C.; Zapol, P.; Curtiss, L. A.; Raghavachari, K. *J. Chem. Phys.* **2000**, *104*, 5850.
(12) Johnson, B. G.; González, C.; Gill, P. M. W.; Pople, J. A. *Chem. Phys. Lett.* **1994**, *221*, 100.
(13) Pederson, M. R. *Chem. Phys. Lett.* **1994**, *230*, 54.
(14) Porezag, D.; Pederson, M. R. *J. Chem. Phys*. **1995**, *102*, 9345.
(15) Durant, J. L. *Chem. Phys. Lett.* **1996**, *256*, 595.
(16) Jursic, B. S. *Chem. Phys. Lett.* **1997**, *264*, 113.
(17) Skokov, S.; Wheeler, R. A. *Chem. Phys. Lett.* **1997**, *271*, 251.
(18) Tozer, D. J.; Handy, N. C. *J. Phys. Chem. A* **1998**, *102*, 3162.
(19) Proynov, E.; Chermette, H.; Salahub, D. R. *J. Chem. Phys*. **2000**, *113*, 10021.
(20) Lynch, B. J.; Truhlar, D. G. *J. Phys. Chem. A* **2001**, *105*, 2936.
(21) Lynch, B. J.; Fast, P. L.; Harris, M.; Truhlar, D. G. *J. Phys. Chem. A* **2000**, *104*, 21.
(22) Warshel, A.; Levitt, M. *J. Mol. Biol.* **1976**, *103*, 227.
(23) Singh, U. C.; Kollman, P. A. *J. Comput.Chem.* **1986**, *7*, 718.
(24) Field, M. J.; Bash, P. A.; Karplus, M. *J. Comput. Chem.* **1990**, *11*, 700.
(25) Eckert, J.; Kubas, G. J.; Hall, J. H.; Hay, P. J.; Boyle, C. M. *J. Am. Chem. Soc.* **1990**, *112*, 2324.
(26) Warshel, A. *Computer Modeling of Chemical Reactions in Enzymes and Solutions*; J. Wiley & Sons: New York, 1991.
(27) Kawamura, H.; Koga, N.; Morokuma, K. *J. Am. Chem. Soc.* **1992**, *114*, 8687.
(28) Maseras, F.; Koga, N.; Morokuma, K. *Organometallics* **1994**, *13*, 4008.
(29) Maseras, F.; Morokuma, K. *J. Comput.Chem.* **1995**, *16*, 1170.
(30) Humbel, S.; Sieber, S.; Morokuma, K. *J. Chem. Phys.* **1996**, *105*, 1959.
(31) Svensson, M.; Humbel, S.; Morokuma, K. *J. Chem. Phys.* **1996**, *105*, 3654.
(32) Svensson, M.; Humbel, S.; Froese, R. D. J.; Matsubara, T.; Sieber, S.; Morokuma, K. *J. Phys. Chem.* **1996**, *100*, 19357.
(33) Coitiño, E. L.; Truhlar, D. G.; Morokuma, K. *Chem. Phys. Lett.* **1996**, *259*, 159.
(34) Coitiño, E. L.; Truhlar, D. G. *J. Phys. Chem. A* **1997**, *101*, 4641.
(35) Noland, M.; Coitiño, E. L.; Truhlar, D. G. *J. Phys. Chem. A* **1997**, *101*, 1193.
(36) Gao, J. *Rev. Comput. Chem.* **1996**, *7*, 119.
(37) Corchado, J. C.; Truhlar, D. G. *J. Phys. Chem. A* **1998**, *102*, 1895.
(38) Corchado, J. C.; Truhlar, D. G. In *Combined Quantum Mechanical and Molecular Mechanical Methods*; Gao, J., Thompson, M. A., Eds.; ACS Symposium Series, Vol. 712; American Chemical Society: Washington, DC, 1998; p 106.
(39) Dapprich, S.; Komaromi, I.; Byun, K. S.; Morokuma, K.; Frisch, M. J. *J. Mol. Struct. (THEOHEM)* **1999**, *461*, 1.
(40) Espinosa-García, J. *Phys. Chem. Chem. Phys*., in press.
(41) Zhang, Y.; Liu, H.; Yang, W. *J. Chem. Phys.* **2000**, *112*, 3483.
(42) Truong, T. N.; Duncan, W. T.; Tirtowidjojo, A. *Phys. Chem. Chem. Phys.* **1999**, *1*, 1061.
(43) Truong, T. N.; Truong, T.-T. *Chem. Phys. Lett.* **1999**, *314*, 529.
(44) Truong, T. N.; Maity, D. K.; Truong, T.-T. *J. Chem. Phys.* **2000**, *112*, 24.
(45) Espinosa-García, J.; Corchado, J. C. *J. Chem. Phys.* **2001**, *115*, 3021.
(46) Truhlar, D. G.; Isaacson, A. D.; Garrett, B. C. In *The Theory of Chemical Reactions*; Baer, M., Ed.; Chemical Rubber Co.: Boca Raton, FL, 1985; Vol. 4.
(47) Bondi, D. K.; Connor, J. N. L.; Garrett, B. C.; Truhlar, D. G. *J. Chem. Phys.* **1983**, *78*, 5981.
(48) Clyne, M. A. A.; Holtz, P. M. *J. Chem. Soc., Faraday Trans 2* **1979**, *75*, 582.
(49) Martin, J. P.; Paraskevopoulos, G. *Can. J. Chem.* **1983**, *61*, 861.
(50) Talukdar, R.; Mellouki, A.; Gierczak, T.; Burkholder, J. B.; McKeen, S. A.; Ravishankara, A. R. *J. Phys. Chem.* **1991**, *95*, 5815.
(51) Hsu, K. J.; DeMoore, W. B. *J. Phys. Chem.* **1995**, *99*, 1235.
(52) Orkin, V. L.; Huie, R. E.; Kurylo, M. J. *J. Phys. Chem.* **1996**, *100*, 8907.
(53) DeMore, W. B.; Sander, S. P.; Golden, D. M.; Hampson, R. F.; Kurylo, M. J.; Howard, C. J.; Ravishankara, A. R.; Kolb, C. E.; Molina, M. Chemical Kinetics and Photochemical Data for Use in Stratospheric Modeling. JPL Publication 94-26; JPL: Pasadena, CA, 1994.
(54) Jeong, K.-M.; Kaufman, F. *J. Phys. Chem.* **1982**, *86*, 1816.
(55) Cohen, N.; Benson, S. W. *J. Phys. Chem.* **1987**, *91*, 162.
(56) Frisch, M. J.; Trucks, G. W.; Schlegel, H. B.; Scuseria, E.; Robb, M. A.; Cheeseman, J. R.; Zakrzewski, V. G.; Montgomery, J. A.; Stratman, R. E.; Burant, J. C.; Dapprich, S.; Millam, J. M.; Daniels, A. D.; Kudin, K. N.; Strain, M. C.; Farkas, O.; Tomasi, J.; Barone, V.; Cossi, M.; Cammi, R.; Menucci, B.; Pomelli, C.; Adamo, C.; Clifford, S.; Ochterki, J.; Petterson, G. A.; Ayala, P. Y.; Cui, Q.; Morokuma, K.; Malik, D. K.; Rabuk, A. D.; Raghavachari, K.; Foresman, J. B.; Cioslowski, J.; Ortiz, J. V.; Stefanov, J. J.; Liu, G.; Liashenko, A.; Piskorz, P.; Komaromi, I.; Gomperts, R.; Martin, R. L.; Fox, D. J.; Keith, T.; Al-Laham, M. A.; Peng, C. Y.; Nanayakkara, A.; González, C.; Challacombe, M.; Gill, P. M. W.; Johnson, B. G.; Chen, W.; Wong, M. W.; Andres, J. L.; Head-Gordon, M.; Reploge, E. S.; Pople, J. A. *Gaussian98*, Revision A.7; Gaussian Inc.: Pittsburgh, PA, 1998.
(57) Bartlett, R. J. *J. Phys. Chem*. **1989**, *93*, 1697.
(58) Kendall, R. A.; Dunning, T. H.; Harrison, R. J. *J. Chem. Phys*. **1992**, *96*, 6796.
(59) Stephens, P. J.; Devlin, F. J.; Chabalowski, C. F.; Frich, M. K. *J. Phys. Chem*. **1994**, *98*, 11623.
(60) Becke, A. D. *J. Chem. Phys.* **1993**, *98*, 5648.
(61) Lee, C.; Yang, W.; Parr, R. G. *Phys. Rev. B* **1988**, *37*, 785.
(62) Isaacson, A. D.; Truhlar, D. G. *J. Chem. Phys*. **1982**, *76*, 1380.
(63) Miller, W. H.; Handy, N. C.; Adams, J. E. *J. Chem. Phys*. **1980**, *72*, 99.
(64) Morokuma, K.; Kato, S. In *Potential Energy Surfaces and Dynamics Calculations*; Truhlar, D. G.; Plenum: New York, 1981; p 243.
(65) Kraka, E.; Dunning, T. H. In *Advances in Molecular Electronic Structure Theory*; JAI: New York, 1990; Vol. I, p 129.

(66) Garrett, B. C.; Truhlar, D. G. *J. Am. Chem. Soc*. **1979**, *101*, 4534.
(67) Corchado, J. C.; Coitiño, E. L.; Chuang, Y.-Y.; Truhlar, D. G. *GAUSSRATE*, Version 8.0/P8.0-G94; University of Minnesota: Minneapolis, MN, 1998.
(68) Chuang, Y. Y.; Corchado, J. C.; Fast, P. L.; Villá, J.; Coitiño, E. L.; Hu, W. P.; Liu, Y. P.; Lynch, G. C.; Nguyen, K.; Jackells, C. F.; Gu, M. Z.; Rossi, I.; Clayton, S.; Melissas, V.; Steckler, R.; Garrett, B. C.; Isaacson, A. D.; Truhlar, D. G. *POLYRATE*, Version 8.4; University of Minnesota: Minneapolis, 1999.
(69) Truhlar, D. G. *J. Comput. Chem*. **1991**, *12*, 266.
(70) Jackels, C. F.; Gu, Z.; Truhlar, D. G. *J. Chem. Phys*. **1995**, *102*, 3188.
(71) Chuang, Y. Y.; Truhlar, D. G. *J. Phys. Chem. A* **1997**, *101*, 3808.
(72) Natanson, G. A.; Garrett, B. C.; Truong, T. N.; Joseph, T.; Truhlar, D. G. *J. Chem. Phys*. **1991**, *94*, 7875.
(73) Espinosa-García, J.; Corchado, J. C. *J. Phys. Chem.* **1996**, *100*, 16561.
(74) Corchado, J. C.; Espinosa-García, J. *J. Chem. Phys*. **1997**, *106*, 4013.
(75) Lu, D.h.; Truong, T. N.; Melissas, V. S.; Lynch, G. C.; Liu, Y. P.; Garrett, B. C.; Steckler, R.; Isaacson, A. D.; Rai, S. N.; Hancock, G. C.; Lauderdale, G. C.; Joseph, T.; Truhlar, D. G. *Comput. Phys. Commun*. **1992**, *71*, 235.
(76) Truong, T. N.; Lu, D.-h.; Lynch, G. C.; Liu, Y. P.; Melissas, V. S.; Stewart, J. J.; Steckler, R.; Garrett, B. C.; Isaacson, A. D.; González-Lafont, A.; Rai, S. N.; Hancock, G. C.; Joseph, T.; Truhlar, D. G. *Comput. Phys. Commun*. **1993**, *75*, 43.
(77) Beagley, B.; Jones, M. O.; Zanjanchi, M. A. *J. Mol. Struct.* **1979,** *56*, 215.
(78) Pauling, L. *J. Chem. Phys.* **1969**, *51*, 2767.
(79) Espinosa-García, J.; Olivares del Valle, F. J.; Leroy, G.; Sana, M.; Wilante, C. *J. Mol. Struct. (THEOCHEM)* **1992,** *258*, 315.
(80) Hammond, G. S. *J. Am. Chem. Soc*. **1955**, *77*, 334.
(81) Wu, E. C.; Rodgers, A. S. *J. Phys. Chem*. **1974**, *78*, 2315.
(82) Dixon, D. A.; Feller, D. *J. Phys. Chem. A* **1998**, *102*, 8209.
(83) Fast, P. L.; Corchado, J. C.; Sánchez, M. L.; Truhlar, D. G. *J. Phys. Chem. A* **1999**, *103*, 3139.
(84) Malik, D. K.; Petersson, G. A.; Montgomery, J. A. *J. Chem. Phys.* **1998**, *108*, 5704.
(85) Aliagas, I.; Gronert, S. *J. Phys. Chem. A* **1998**, *102*, 2609.
(86) Korchowiec, J.; Kawakara, S. I.; Matsumura, K.; Uchimaru, T.; Surgie, M. *J. Phys. Chem. A* **1999**, *103*, 3548.
(87) Masgrau, L.; González-Lafont, A.; Lluch, J. M. *J. Chem. Phys.* **2001**, *114*, 2154.
(88) Lynch, B. J.; Truhlar, D. G. *J. Chem. Phys*. **2002**, *106*, 842.
(89) Basch, H.; Hoz, S. *J. Phys. Chem. A* **1997**, *101*, 4416.
(90) Wheeler, M. D.; Tsiouris, M.; Laster, M.; Lendvay, G. *J. Chem. Phys*. **2000**, *112*, 6590.
(91) Espinosa-García, J.; Corchado. J. C. *J. Chem. Phys.* **1994**, *101*, 8700.
(92) Espinosa-García, J.; Coitiño, E. L.; González-Lafont, A.; Lluch, J. M. *J. Phys. Chem. A* **1998**, *102*, 10715.
(93) Espinosa-García, J.; Corchado. J. C. *J. Chem. Phys.* **1994**, *101*, 1333.
(94) Espinosa-García, J. *J. Phys. Chem. A* **2000**, *104*, 7537.
(95) Melissas, V. S.; Truhlar, D. G. *J. Chem. Phys.* **1993**, *99*, 1013.
(96) Espinosa-García, J.; Corchado. J. C. *J. Chem. Phys.* **2000**, *112*, 5731.
(97) Prather, M.; Spivakovsky, C. M. *Geophys. Res.* **1990**, *95*, 723.
(98) Francisco, J. S. *J. Chem. Phys.* **1992**, *96*, 7597.
(99) Atkinson, R. *Chem. Rev*. **1985**, *85*, 192.